

Estimation of slip rates in the southern Tien Shan using cosmic ray exposure dates of abandoned alluvial fans

Erik Thorson Brown* } Centre de Spectrométrie Nucléaire et de Spectrométrie de Masse, CNRS-IN₂P₃, Bâtiment 108,
Didier L. Bourlès } F-91405 Campus Orsay, France

B. Clark Burchfiel } Department of Earth, Atmospheric and Planetary Sciences, Massachusetts Institute of Technology,
Cambridge, Massachusetts 02139

Deng Qidong } Institute of Geology, State Seismology Bureau, Beijing, China

Li Jun } Provincial Bureau of Seismology, State Seismology Bureau, Urumqi, Xinjiang, China

Peter Molnar } Department of Earth, Atmospheric and Planetary Sciences, Massachusetts Institute of Technology,
Cambridge, Massachusetts 02139

Grant M. Raisbeck } Centre de Spectrométrie Nucléaire et de Spectrométrie de Masse, CNRS-IN₂P₃, Bâtiment 108,
Françoise Yiou } F-91405 Campus Orsay, France

ABSTRACT

Cosmic ray exposure dates (based on in situ-produced ¹⁰Be), in combination with measured heights of fault scarps that cut three abandoned fans, imply a slip rate of less than ~2 mm/yr on the bounding thrust fault along a segment of the southern flank of the Tien Shan of central Asia. This rate, somewhat lower than those for the segment farther west and for the northern margin of the belt, implies that the distribution of shortening across the Tien Shan must change markedly along the belt. The date of abandonment of the smallest of the three fans is consistent with fan formation since the last glacial maximum, but the other two fans appear to have been formed and abandoned prior to that time. These and other results suggest that advances and retreats of alpine glaciers may not be synchronized with continental ice sheets and that not all prominent geomorphological features in arid Asian regions have formed since the last glacial maximum.

In this study we have assessed the relationship between cosmogenic nuclide content of individual clasts and the time since their deposition on a surface. Cosmogenic nuclide accumulation represents the integrated total

surface exposure of rocks in source regions during transport and since deposition. Post-depositional processes (erosion, burial, bioturbation, and cryoturbation), all of which decrease the quantity of cosmogenic nuclides produced in a rock in a given time and hence the apparent exposure age, also cause significant scatter among apparent ages of samples from the surfaces. Very low ¹⁰Be concentrations in material from active streambeds and at depth below one of the fan surfaces indicate that exposure prior to deposition onto fan surfaces was minimal (<~2000 yr); it follows that the dates for individual clasts are lower limits for the time since abandonment of the fans. Because such dates place lower bounds on the time since initiation of scarp preservation, the associated slip rates should represent upper limits.

INTRODUCTION

Among active intracontinental mountain belts, the Tien Shan of central Asia is the highest and most active. This east-west-trending belt is nearly 2000 km long and consists of high ranges separated by linear sedimentary basins filled with as much as 1–2 km of Cenozoic debris (Fig. 1) (Sadybakasov, 1990). Thrust or reverse slip on faults dipping from the edges of the basins beneath the ranges has created the basin-and-range landscape (Makarov, 1977; Sadybakasov, 1990).

Fault-plane solutions of virtually all earthquakes demonstrate such faulting, and locations of earthquakes confirm that deformation occurs throughout the range. The region has high relief; both the highest mountain outside the Himalaya-Karakorum region (Peak Pobedy, 7439 m, on the border of Kyrgyzstan and Xinjiang) and the second lowest region in the world (the Turfan depression, –154 m) are within the Tien Shan. Three earthquakes in this century were assigned magnitudes greater than 8, and at least two from the previous century demonstrated a high level of seismicity (e.g., Molnar and Deng, 1984; Richter, 1958).

The simple aspects of the topography and the style of deformation reveal a linear character, suggesting the creation of a classical two-dimensional mountain belt, but there are obscure marked variations along the belt. The underlying upper mantle structure, inferred from gravity anomalies (Burov et al., 1990), seismic anisotropy (Makeyeva et al., 1992), and P-wave traveltimes (Roecker et al., 1993), suggests that there is as much variation along the belt as across it. Major strike-slip faults obliquely cross the Tien Shan and divide the belt into segments of different widths. Moreover, some segments of the Tien Shan are bounded by clearly active fold-and-thrust belts, where sedimentary rock has been detached from the underlying basement (e.g., Avouac et al., 1993; Burchfiel, et al. in press; Feng et al., 1991; Molnar et al., 1994). Along other parts, however, the mountains rise

*Present address: Large Lakes Observatory, University of Minnesota, Duluth, Minnesota 55812; e-mail: etbrown@d.umn.edu.

abruptly from the edges of the neighboring Tarim and Dzhungarian basins, indicating active thrust faulting of the range over the adjacent areas. As a result of this variety, the Tien Shan has a spectrum of structures that individually are worthy of study.

The rapid deformation and variety of structure and style of deformation of the Tien Shan make it the outstanding laboratory for the study of intra-continental mountain building and for the study of seismic hazards in such settings. A major motivation for our work in the Tien Shan derives from its similarity in style and rate of deformation to the Transverse Ranges of California. This study was conceived both as a part of a larger endeavor to constrain the overall rate of shortening across the belt and as a study of active reverse faulting along its margin.

Both the fault-plane solutions of earthquakes and the surface geology at the margins of the Tien Shan suggest that fault planes dip at roughly 15° – 45° beneath the range. In general, active faults do not mark the contact of the pre-Cenozoic rock with the late Cenozoic sediments in the adjacent basins. Where we have seen pre-Cenozoic rock, both on the northern and southern sides of the range, it dips steeply (30° – 40°) toward the adjacent Tarim, or Dzhungarian, basin. Thus, this pre-Cenozoic rock seems to have been folded over a ramp anticline and is above the segment of the thrust fault that dips gently beneath the edge of the belt (Fig. 2). In two places, one on the north side and the other on the south side of the Tien Shan, Burchfiel et al. (in press) mapped inactive but young faults at the contacts between pre-Cenozoic and older Quaternary rocks at the range fronts. In both places the fault dips about 40° beneath the range. Where a fold and thrust belt bounds the range, slip on the flat part of the thrust fault has detached the sedimentary cover from the basement of the Tarim (or Dzhungarian) basin (e.g., Avouac et al., 1993; Burchfiel et al., in press). The width of the belt where Mesozoic and Cenozoic sedimentary rocks have been detached and folded is commonly 20–40 km. Where no fold-and-thrust belt is present, an active scarp crops out near the edge of the pre-Cenozoic rock, 1–2 km from it, but not at the contact between them.

We concentrated on a segment of the southern edge of the Tien Shan where prominent scarps cross fans that show evidence of deposition by both alluvial and debris-flow processes (Figs. 3 and 4) but little evidence of deposition of eolian silt. We saw only one fresh scarp throughout the length of this segment, indicating that the main thrust fault beneath the edge of the belt has reached the surface as a single fault surface, and not as a set of splays. Thus, a quantification of the rate of offset on the fault provides a constraint on the rate at which the Tarim basin is being under-

thrust beneath the southern margin of the Tien Shan at this locality.

SAMPLING AND ANALYSES

The steps toward estimating a rate of underthrusting, and hence a fraction of the overall convergence rate, consist of (1) quantifying the vertical component of displacement, (2) dating alluvial fans that have been offset by faults, and (3) estimating the dip of the fault for calculation of a hor-

izontal rate from the vertical rate. The first of these is relatively straightforward. Dating the fans requires quantification of a number of uncertainties and considerable attention. Much of this study examines residence times of cobbles and boulders in high-energy environments before deposition into the fans, and erosion rates of fans in desert environments. Uncertainties in the dip of the faults responsible for the scarps we measured result in an uncertainty of a factor of at least two in the rate of underthrusting.

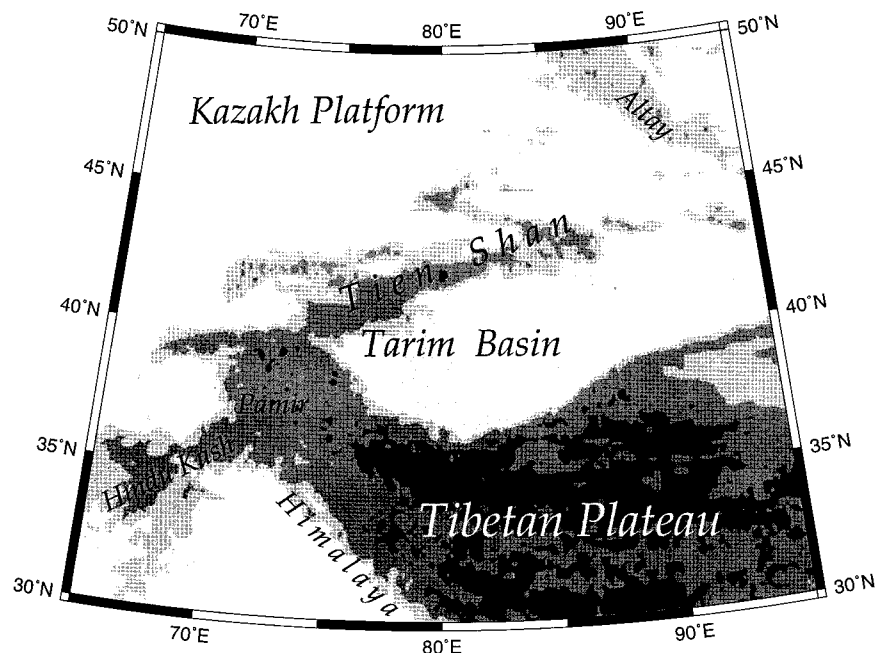


Figure 1. Map of central Asia showing the Tien Shan and its surroundings.

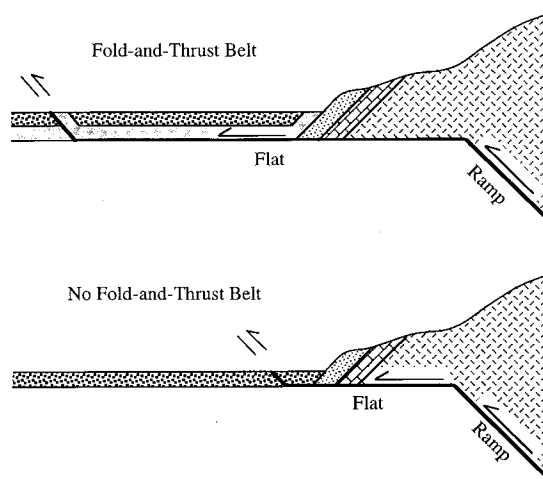


Figure 2. Sketch contrasting the situation of our field site with that of a fold-and-thrust belt.

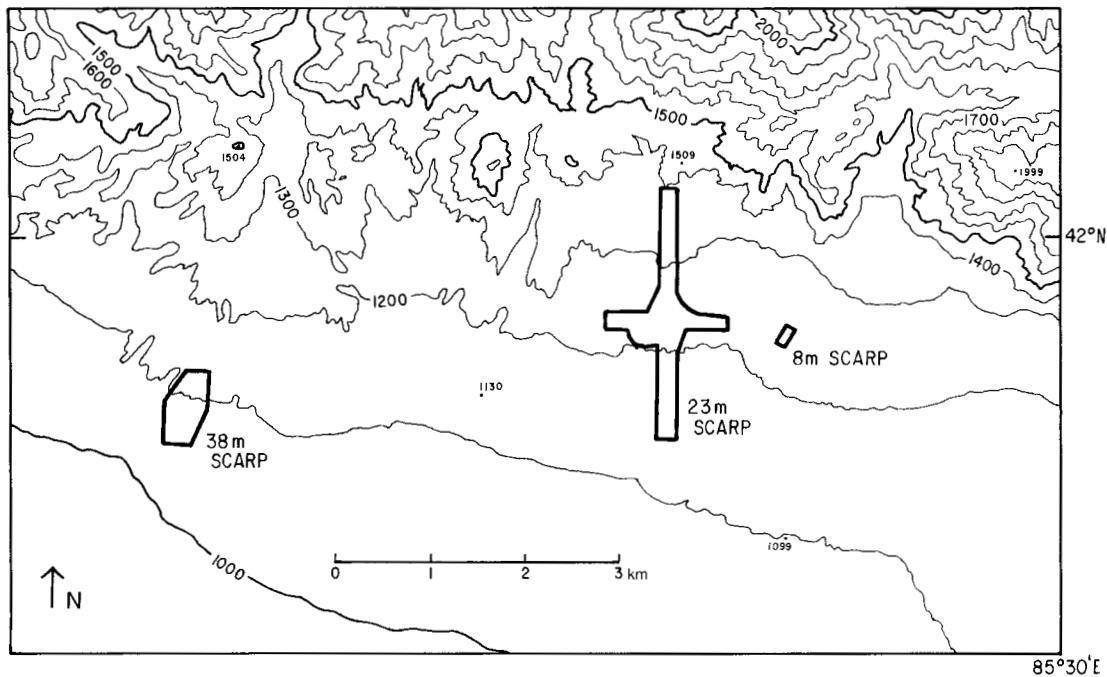


Figure 3. Topographical map of the region of this study. The areas of the three fans surveyed are outlined.

Total Station Measurements

Heights of Scarps. We constructed topographic maps and profiles of portions of three fans cut by fault scarps (Figs. 5A, 6A, and 7A). All three fans are largely inactive; major streams have incised into them and isolated the fan surfaces from active stream erosion and deposition. We used a total station, a combination of theodolite and distance ranging device, to map the fans and scarps. Uncertainties in horizontal positions and heights of surveyed points are a few centimeters, negligible compared with small-scale relief on the fans.

We concentrated our efforts on one fan (the central fan), the largest of the three we studied (Fig. 5). At this site we constructed two long, parallel profiles from the range front to the southern edge of the inactive fan. We also mapped in detail a section approximately 250 m by 500 m, in order to define the variation in topography on both the fan and the scarp (Fig. 5, B and C). We then constructed a number of short profiles across the scarp to define the trace of the fault, which is not linear. Active streams currently erode the regions east and west of the sections mapped in Figure 5A.

We mapped two other abandoned fans, one approximately 600 m to the east (Fig. 6), and the other (Fig. 7) approximately 5 km west of the central fan. We noted in the field that the character of

the surface of the eastern fan differed from that of the central fan; its rougher texture suggests that this smaller fan is younger. The western fan (Figs. 2 and 7) probably represents only a small fraction of what may have been a much larger fan. For the eastern and western fans, and for the areas outside of the detailed survey in Figure 5C, we did not make an effort to define relief on the fans except at the scarp. Instead, we measured heights only on broad crests of the low, flat ridges between the gullies that have cut into the fans. The areas encompassed by the latter two surveys cover essentially the entire remnants of the fans, so that the boundaries of the mapped areas mark the edges of the areas not eroded by active streams.

To estimate vertical components of offset, we constructed profiles perpendicular to the scarps for all three fans. Long profiles across the central fan reveal some relief on the fan above and below the fault scarp (Fig. 5B). Nevertheless, the vertical offset of 23 (± 2) m is well constrained. Relief is large at the scarp, because of both the offset and significant erosion of the fan (Fig. 5, B and C). The topography of this fan commonly varies by 2–4 m over distances of 50 m; gullies are as deep as 10 m near the scarp. Hence, although active streams do not cross the segments of fans that we mapped, there must have been some incision of the fans by ephemeral streams after the major streams emanating from the adjacent mountains abandoned the fans. The morphology of the

scarps shows no indication of evolution toward a smooth profile by gradual transfer of material at rates proportional to local slope, and therefore obeys the diffusion equation (e.g., Hanks et al., 1984). For this reason we made no effort to apply error-function solutions to topographic profiles to estimate rates of scarp evolution or dates of initiation of faulting. Profiles across the eastern fan demonstrate a vertical component of displacement of 8.2 (± 0.5) m (Fig. 6B). The surface of the western fan dips in a direction oblique to the trend of its scarp, and its northwestern and southeastern margins have been destroyed by erosion. A profile, nevertheless, yields a vertical offset of 38 (± 2) m (Fig. 6C).

Dips of Faults. Inferring either a horizontal component of displacement, or a component parallel to the dip of the fault, requires an estimate of the dip of the fault near the surface. The available data may be used to place bounds on, but not make accurate estimates of, such dips. In principle, if a planar fault surface intersects the irregular surface of the Earth, the trace of the scarp can define the orientation of the plane. Specifically, a planar fault dipping northward beneath landforms having a regional dip to the south will produce a scalloped surface trace that curves southward over the highest terrain and northward into the lowest terrain.

The trace of the scarp we studied is irregular and clearly does not display such characteristics.

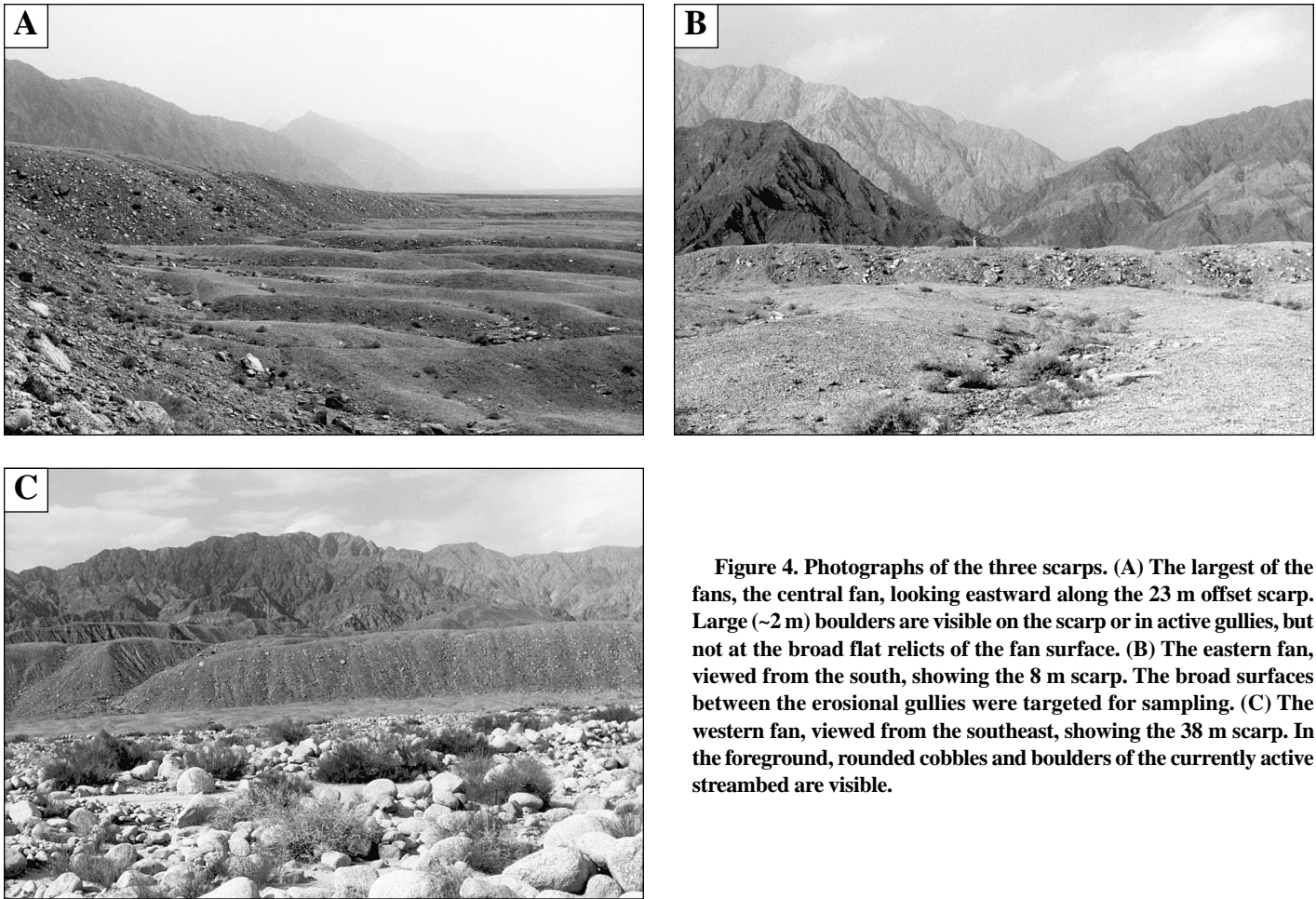


Figure 4. Photographs of the three scarps. (A) The largest of the fans, the central fan, looking eastward along the 23 m offset scarp. Large (~2 m) boulders are visible on the scarp or in active gullies, but not at the broad flat relicts of the fan surface. (B) The eastern fan, viewed from the south, showing the 8 m scarp. The broad surfaces between the erosional gullies were targeted for sampling. (C) The western fan, viewed from the southeast, showing the 38 m scarp. In the foreground, rounded cobbles and boulders of the currently active streambed are visible.

The fault crosses a relatively low-lying region between the central and eastern fan segments (Fig. 5A). Within that region we mapped an area ($x \approx 1460$ m, $y \approx 1000$ m, in Fig. 5A) where we recognized a small fragment of the ~8 m scarp associated with the eastern fan. At this low point no curvature to the north could be seen. Thus, we conclude that, at least near the surface, the fault trace cannot be planar. If the fault surface were corrugated, and slip were parallel to the corrugations, the intersection of the fault with the Earth's surface could form the irregular trace that we observe. However, justifying such an assumption would be difficult, and determining the slip vector would be virtually impossible.

Other facts constrain possible dips of the fault. Fault-plane solutions of earthquakes in the Tien Shan show typical dips, δ , of $\sim 15^\circ$ – 45° (Ekström, 1987; Nelson et al., 1987; Ni, 1978; Shirokova, 1967, 1974; Tapponnier and Molnar, 1979). Nelson et al. (1987) inferred $\delta = 41^\circ$ for an event ~75 km west of our study area, the only earthquake within 100 km for which we have found a reliable solution. Moderate and large earthquakes

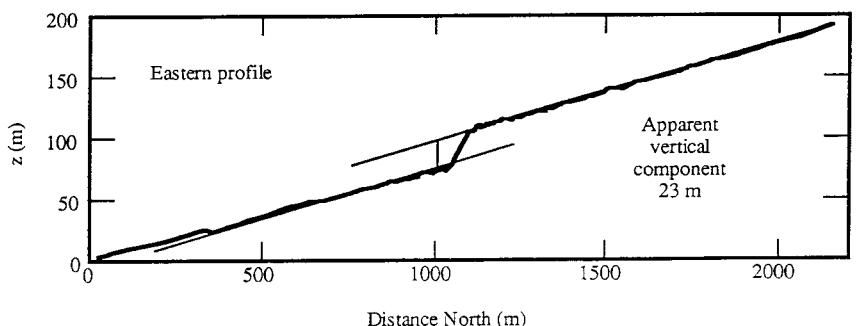
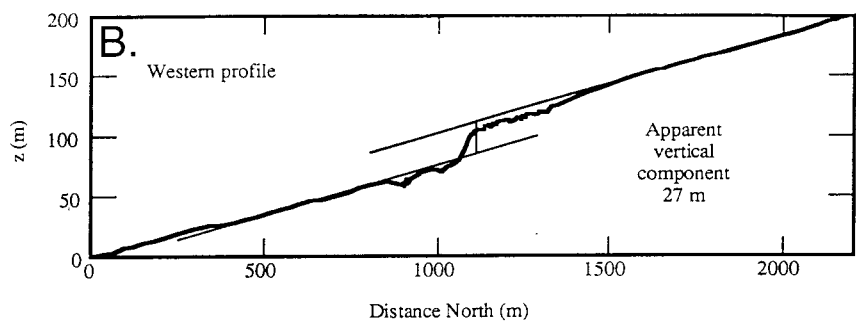
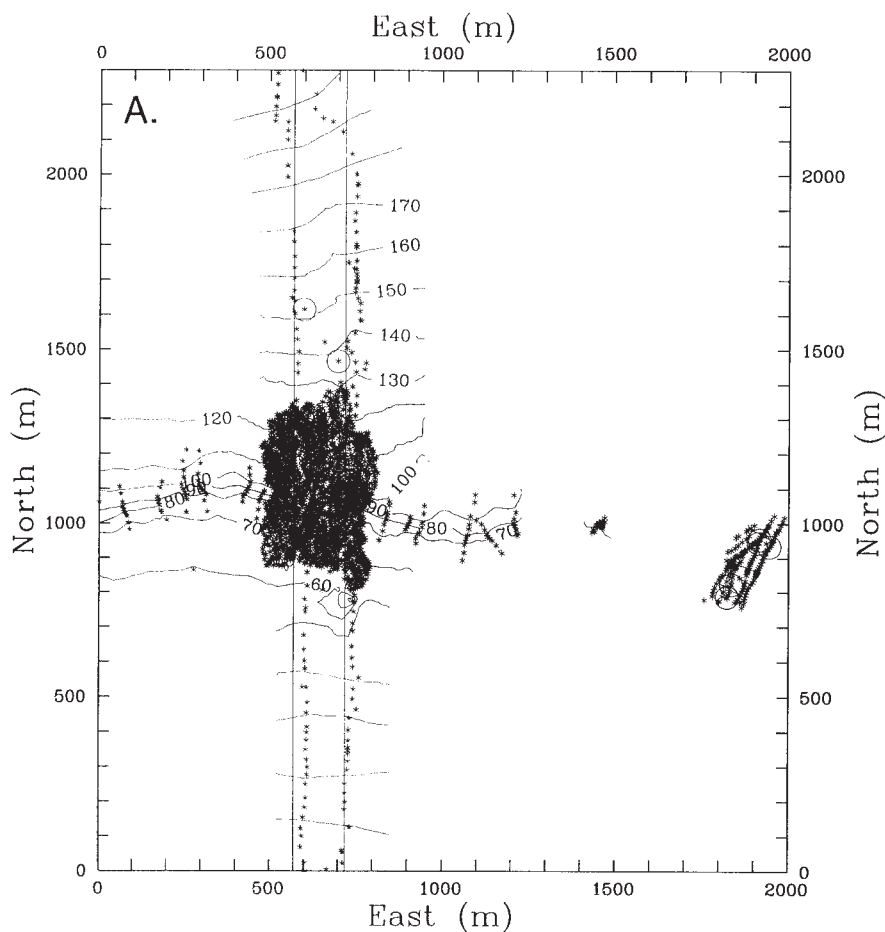
apparently occur beneath the pre-Cenozoic rock of the Tien Shan, and the faults activated by such earthquakes appear to dip more steeply beneath the mountains than near the edge of the ranges (e.g., Avouac et al., 1993; Burchfiel et al., in press). Thus, the faults that have created scarps at the surface should dip more gently than 45° .

In fold-and-thrust belts, thrust faults commonly are parallel to bedding planes, which in turn have been flexed down toward the range. On the north side of the Tien Shan, balanced cross sections across the range suggest dips of the basement of about 5° (Burchfiel et al., in press). In the parts of the south side where no fold-and-thrust belt has developed, but the basement has been flexed down 6–8 km (Terman et al., 1967), the basement must dip at least as steeply as 5° , and any fault emanating from that surface must dip more steeply.

Thus, given an absolute lower bound of 5° and an upper bound of 45° , we assumed an average value of $\delta = 14.5^\circ$ with a range of 9.5° to 30° ; this makes calculations simple, because $(\sin \delta)^{-1} = 4 \pm 2$.

Cosmic Ray Exposure Dates

Theory. On Earth, cosmogenic nuclides (including ^3He , ^{10}Be , ^{14}C , ^{21}Ne , ^{26}Al , ^{36}Cl) are produced by nuclear reactions induced by interaction of high energy cosmic rays and terrestrial matter. Such reactions occur not only in the atmosphere but also in situ within mineral lattices of rock exposed at the Earth's surface. Quartz is a particularly appropriate mineral for cosmic ray exposure dating using ^{10}Be and ^{26}Al . It is abundant, easily isolated and dissolved in the laboratory, and is a compositionally simple mineral with a minimal number of targets for spallation reactions (Lal and Arnold, 1985; Yiou et al., 1984). The exponential attenuation of cosmic ray neutrons by matter essentially limits in situ production of these nuclides to a thin skin (a few meters) of the Earth's crust. The accumulation of these nuclides may thus be used for quantitative examination of near-surface exposure histories. In specific cases cosmogenic nuclide concentrations may be used to date events that have brought material to the surface from significant



depths underground (see Cerling and Craig [1994] for a review of this technique).

In general, the concentration of a cosmogenic nuclide, N (atom g^{-1}), at depth x (g cm^{-2}) below a rock surface as a function of time (t), may be represented by

$$N(t) = \frac{Pe^{-xL^{-1}}}{(\epsilon L^{-1} + \lambda)} \left[1 - e^{(\epsilon L^{-1} + \lambda)t} \right] + N(0)e^{-\lambda t} \quad (1)$$

where ϵ is a mass erosion rate ($\text{g cm}^{-2} \text{yr}^{-1}$), P is the production rate (atom $\text{g}^{-1} \text{yr}^{-1}$) at the altitude and latitude of the exposed surface, L is the effective attenuation length of cosmic rays ($\sim 150 \text{g cm}^{-2}$ for production of ^{10}Be [Brown et al., 1992]), λ is the radioactive decay constant (per year), and $N(0)$ is the cosmogenic nuclide concentration at the initiation of the present episode of surface exposure. Depths and lengths are expressed in terms of overlying mass per unit area to eliminate dependence on rock or soil density. This equation assumes constant rates of production and of erosion. Equation 1 has three unknowns: ϵ , t , and $N(0)$. If one assumes that ϵ is negligible, one may calculate a lower limit for the exposure age of a surface, but only if exposure prior to the present episode was minimal [$N(0) \approx 0$]. Assessments of prior exposure to cosmic rays and of erosional processes are critical for quantitative application of this technique.

Strategy for ^{10}Be Sampling. We collected samples for cosmic ray exposure dating from the surfaces of the three abandoned fans. Our working assumption is that when the fan surfaces were active, offsets resulting from movement along the fault were rapidly eliminated by erosion on the upper block and deposition on the lower one. Scarp preservation would have begun with abandonment and incision of fans, presumably due to decreased sediment load and/or increased stream power.

Through our sample collection strategy, we attempted to minimize the effects of postdepositional erosion on the fan surfaces. We sampled quartz-rich rocks at local (on the scale of 5 to 10 m) flat topographic highs where patinas of desert

Figure 5. Maps of the central fan. (A) Topographic map of the central fan including the eastern fan and the small relict fragment of it within the active streambed between the two systems. Areas without measurements have been left blank. Asterisks represent individual triangulation points; circles mark sites of sample collection for ^{10}Be analyses. (B) Two long profiles across the scarp used for estimating the total vertical offset of 23 m for the central fan.

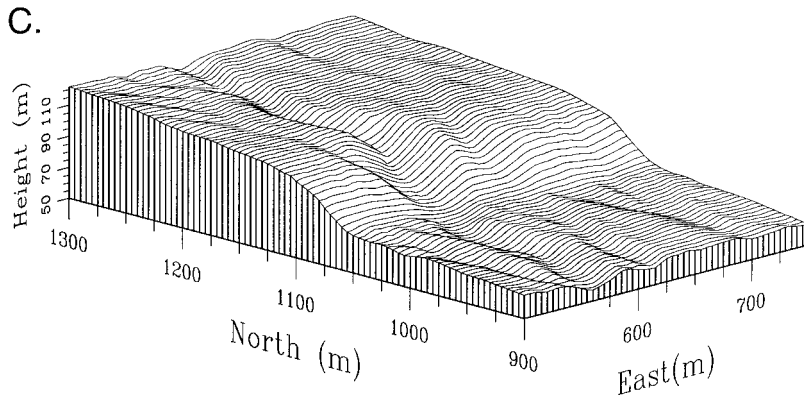


Figure 5. (C) Detailed map of a portion of the scarp in the central fan.

varnish had developed on rock surfaces; we avoided steep slopes adjacent to gullies or fault scarps. Although large (2 m) boulders are exposed midslope in the scarps and gullies, they are no longer present at fan surfaces. Discrete areas of rubble (mostly feldspar phenocrysts) from degraded individual boulders were visible at flat areas of ridge crests between the gullies. At such locations physical erosional processes apparently do not efficiently remove material larger than ~1 or 2 cm. We preferred to sample larger rocks, but the scarcity of quartz-rich rocks with diameters of more than 10 cm meant that most samples were pebbles and cobbles 5 to 10 cm in diameter.

To evaluate the extent of exposure to cosmic rays in the source regions and during transport, we collected samples from the seasonally active streambeds of the rivers that formerly fed the abandoned fans. These samples do not necessarily reflect the erosional conditions at the time that the fans were active, because present-day erosion in source regions may be less intense than at the time of fan deposition. To assess this possibility we also collected samples at approximately 5 m subsurface depth from the walls of the canyon cutting through the central fan. This material was deposited while the fan was active; assuming rapid subsequent burial, it may yield a more reliable estimate of the duration of prior exposure of our samples.

¹⁰Be Analyses. We prepared samples of quartz for determination of ¹⁰Be ($t_{1/2} = 1.5$ m.y.). This nuclide is good for dating studies because its production in near-surface quartz is essentially limited to neutron-induced spallation; it does not suffer from loss by diffusion; and ⁹Be, the stable isotope, is present at extremely low concentrations. Quartz-rich samples were crushed and sieved (0.25–1.0 mm). Other mineral phases were eliminated by selective etching in H₂SiF₆, HCl, and HF. This also eliminated potential sur-

face contamination by ¹⁰Be produced in the atmosphere. The cleaned quartz grains (typically 10–20 g) were then completely dissolved in HF. After addition of 300 μg of ⁹Be carrier, targets of purified Be were prepared for accelerator mass spectrometric (AMS) analyses. Measurements of ¹⁰Be were undertaken at the Tandétron AMS Facility at Gif-sur-Yvette, France (Raisbeck et al., 1987, 1994). Analytical uncertainties (reported throughout as 1s) are based on counting statistics and conservative assumptions of 5% variability in machine response, and a 50% uncertainty in the correction for laboratory and carrier blanks (¹⁰Be:⁹Be ≈ 6 × 10⁻¹⁵). Because of the nature of this study, our strategy, particularly for the low-level samples from active stream beds, was to give priority to analysis of more samples rather than to minimization of analytical uncertainties. Samples from active stream beds had low ¹⁰Be contents, all less than 70 × 10³ atom g⁻¹ (Table 1), in contrast to measured ¹⁰Be concentrations of samples from the three fan surfaces, which range from 234 × 10³ to 634 × 10³ atom g⁻¹ (Table 2).

To calculate ages from ¹⁰Be concentrations we used production rates of 15.4 and of 13.8 atoms g⁻¹ yr⁻¹, for the central and eastern fans and for the western fan, respectively. These rates are based on rates representing ~10 k.y. exposure in the western United States (Nishiizumi et al., 1989) and are normalized to the latitude and altitude of our sites (Lal, 1991). The uncertainties in these production rates may be as great as 15%–20% (Brook and Kurz, 1993; Clark et al., 1995). To a first approximation, uncertainties in production rates result in systematic errors in calculated ages. Rigorous age calculations would require consideration of the temporal variability of production rates; the errors induced in calculated ages by the use of a constant production rate can vary with the age of the surface. For internal comparison of the results from the three surfaces

we utilize ages with uncertainties based only on analytical considerations in terms of ¹⁰Be-years. We also do this to emphasize that, analogous to uncalibrated radiocarbon years, our dates do not represent absolute ages. However, unlike the case of radiocarbon, temporal and spatial variations in ¹⁰Be production rates mean that the relationship between ¹⁰Be years and calendar years will vary from one site to another. This must be considered when comparing cosmic ray exposure dates from different locations. To calculate absolute ages, reported in calendar years, we include a 20% uncertainty in the production rate.

DISCUSSION

Prior Exposure and Postdepositional Processes

The cosmogenic nuclide content of a given rock (Table 2) reflects the rock's entire surface exposure history, integrating its exposure in source regions and during transport, its exposure in the depositional fan and in its current position, and any losses due to radioactive decay (minimal for ¹⁰Be because its half-life is long relative to the rates of processes occurring at this site). All of these processes must be considered in interpretation of cosmogenic nuclide concentrations.

Exposure prior to deposition can be evaluated through the concentrations in clasts within active streambeds (Table 1). The low levels of ¹⁰Be (0–70 × 10³ atom g⁻¹) in these “geological blanks” indicate that, under current erosional conditions, exposure to cosmic rays in source regions and during transport corresponds to <4.5 k.y. of exposure at the altitude of the fans. Comparably low ¹⁰Be concentrations (<3 and 24 × 10³ atom g⁻¹) from the samples taken from the walls of the canyon cutting through the central fan and at depths of ~5 m below the surface similarly indicate minimal exposure prior to deposition onto the active fan and rapid burial after deposition. The relatively smooth convex shapes of the fans suggest that deposition onto each of the fan surfaces was fairly uniform until abandonment, and that abandonment occurred rapidly. These observations imply that the ¹⁰Be that accumulated in the samples from the fan surfaces was produced largely after abandonment of the fans, indicating that the term $N(0)$ from equation 1 is small or negligible, and implying that ¹⁰Be concentrations may be used at this site to place lower limits on exposure ages.

An alternative approach to the problem of using exposure histories of individual clasts to define the timing of deposition and abandonment of a depositional surface utilizes amalgamations of numerous cobbles from the surface to be dated, and of cobbles from depth within that sur-

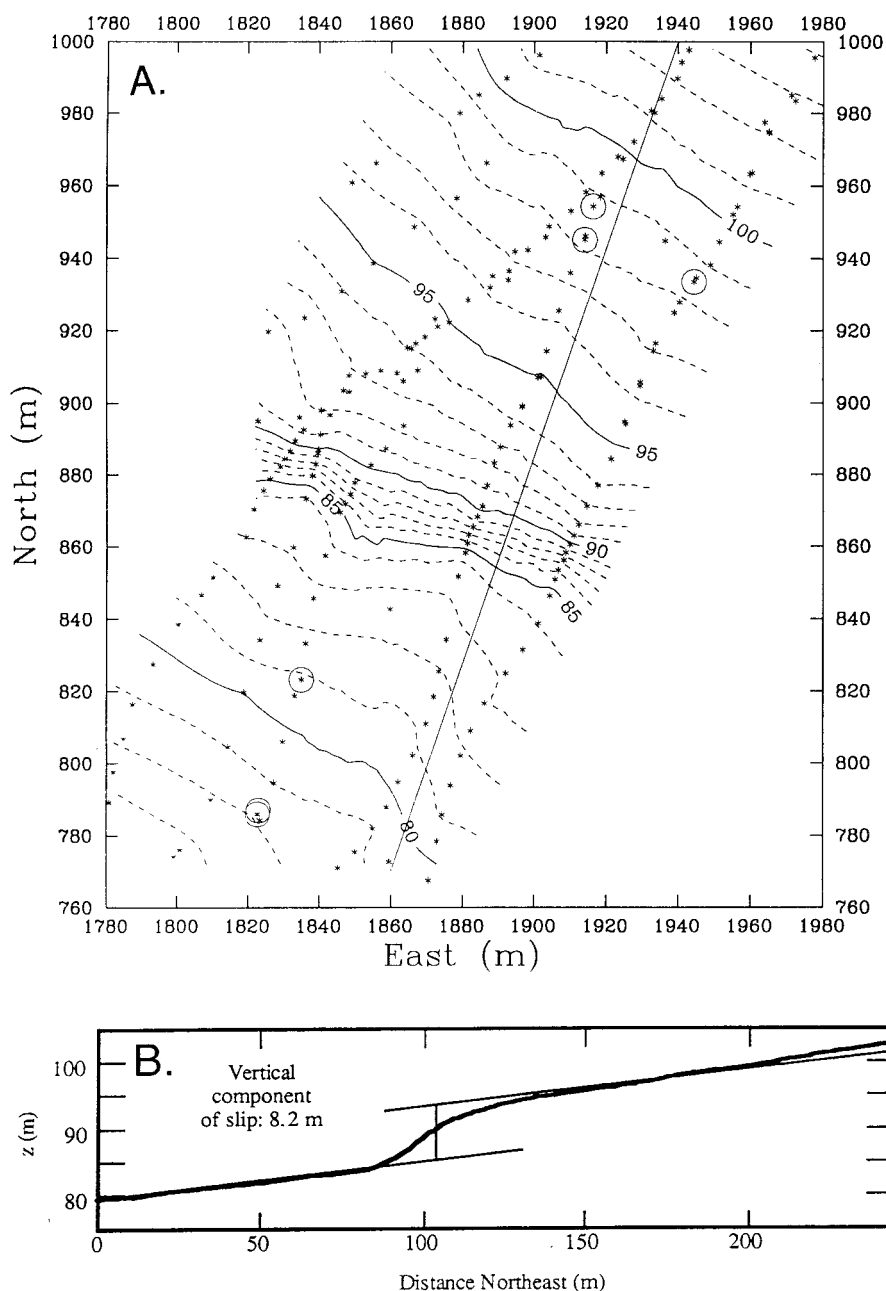


Figure 6. Maps of the eastern fan. (A) Topographic map of the eastern fan. Areas without measurements have been left blank. Asterisks represent individual triangulation points; circles mark sites of sample collection for ^{10}Be analyses. The line represents the axis of the profile shown in B. (B) Profile across the eastern fan constraining offset of the scarp at 8 m.

face (Anderson et al., 1996). The samples taken at depth are analogous to our geological blanks. The amalgamation approach is appropriate for geological settings in which the scatter in cosmogenic nuclide concentrations of rocks on a surface is primarily associated with predepositional processes (variations in total exposure

during exhumation and transport from source regions). However, at locations where postdepositional processes (e.g., burial, erosion, bioturbation, cryoturbation) occur, amalgamation of samples may be inappropriate. All postdepositional processes decrease the quantities of cosmogenic nuclides that accumulate in a surface

rock during a given exposure period. Individual clasts are likely to have been affected differently by these processes. At our sites, where prior exposure makes a relatively small contribution to total cosmogenic nuclide content, the mean age calculated from an amalgamated sample could underestimate the time since fan abandonment, leading to slip rates on the faults that would be too high.

Estimation of Ages and Slip Rates

Our ^{10}Be results show considerable scatter for samples from each of the three fan surfaces. The low values and narrow absolute range of ^{10}Be in the geological blanks relative to these samples (Tables 1 and 2) imply that the scatter observed for each of the fan surfaces is not associated with variable durations of prior exposure, but instead results from postdepositional processes that were not uniform across fan surfaces. The low concentrations in the geological blanks also imply that the exposure ages represent lower limits. It follows that the apparent age of the sample with the highest ^{10}Be concentration most closely approaches the depositional age of the surface. Assuming a geological blank of $25 (\pm 21) \times 10^3$ atom g^{-1} (the mean concentration and standard deviation of the 12 measured samples; equivalent to ~ 2 k.y. exposure on the fans), samples with maximum concentrations give minimum ages of $22 (\pm 3)$, $40 (\pm 3)$, and $35 (\pm 3) \times 10^3$ ^{10}Be yr^{-1} for abandonment of the fans and formation of the scarps; these ages in turn correspond to maximum vertical components of slip rates of $0.37 (\pm 0.11)$, $0.58 (\pm 0.07)$, and $1.09 (\pm 0.11)$ $\text{mm } ^{10}\text{Be}$ yr^{-1} for the eastern, central, and western fans, respectively. Assuming that the fault dips at 14.5° , these values correspond to maximum total rates of slip of $1.5 (\pm 0.4)$, $2.3 (\pm 0.3)$, and $4.4 (\pm 0.4)$ $\text{mm } ^{10}\text{Be}$ yr^{-1} , respectively. The differences among the calculated slip rates for the fans can be reconciled by four lines of reasoning, all of which could be significant at our site.

1. The apparently low age of the western fan (considering the large vertical offset of its scarp) could be explained by more rapid erosion of that surface relative to the other fans. The mean slopes of all three fans, however, are comparable ($\sim 7\%$) and therefore give no evidence of a different process at the western fan.

2. The effects of postdepositional erosional processes on accumulation of cosmogenic nuclides generally increase with the age of a surface. This implies that in a given erosional regime the likelihood that cosmic ray exposure ages underestimate deposition ages increases with the age of the surface. Where prior exposure is minimal, the youngest surface should yield the most accurate slip rate.

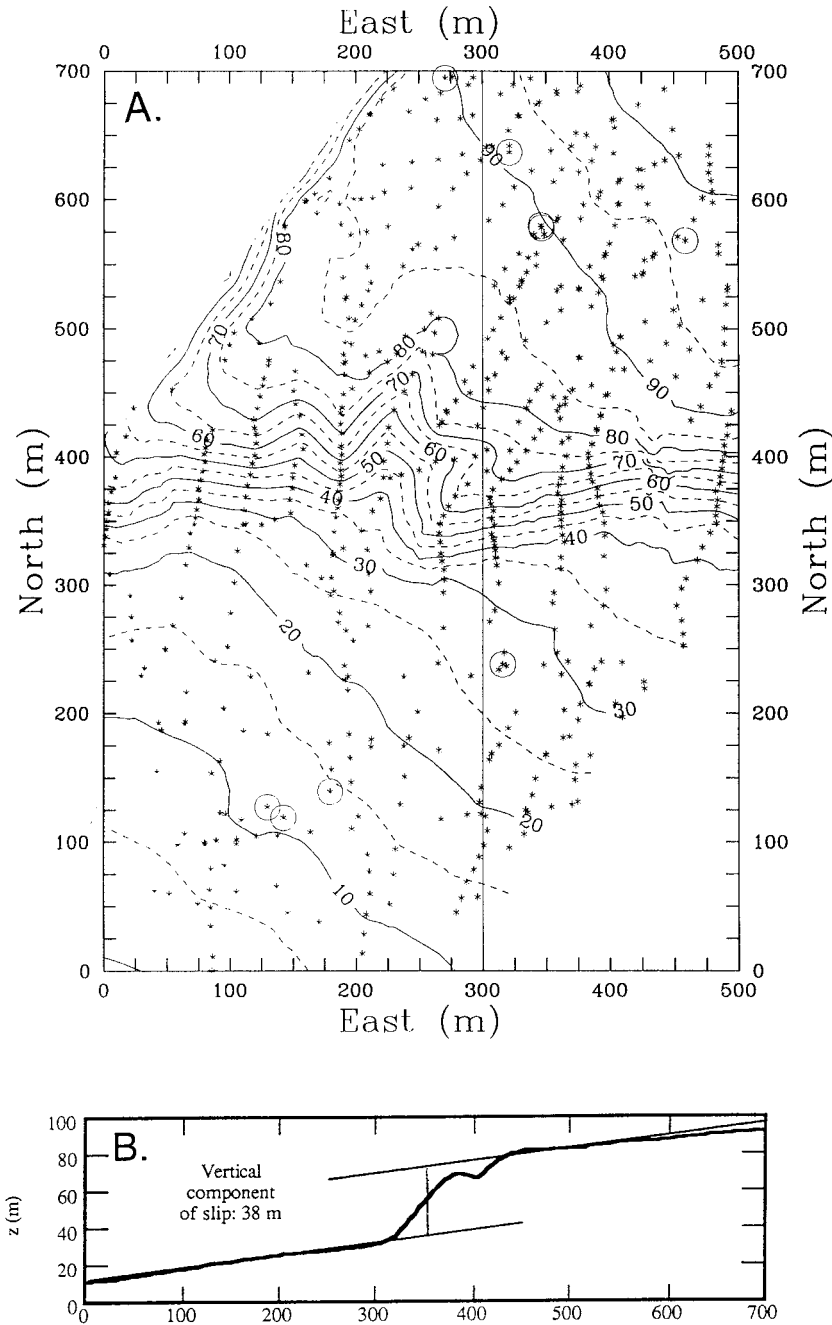


Figure 7. Maps of the western fan. (A) Topographic map of the western fan. Areas without measurements have been left blank. Asterisks represent individual triangulation points; circles mark sites of sample collection for ^{10}Be analyses. The line represents the axis of the profile shown in B. (B) Profile across the western fan constraining offset of the scarp at 38 m.

3. The higher apparent vertical slip rate at the western site could also result from a steeper dip of the fault at the western fan than at the central and eastern fans. For a given convergence rate, a steeper fault corresponds to a more rapid vertical component. Our maps of the traces of the scarps suggest that the dip is not constant along the fault

segment we studied. Furthermore, the dip is not well constrained. Inclusion of a range of dip, which we take to be 9.5° to 30° , in our error propagation yields values of $1.5 (\pm 0.9)$, $2.3 (\pm 1.2)$, and $4.4 (\pm 2.2)$ $\text{mm }^{10}\text{Be yr}^{-1}$ for the net slip rates at the three fans. Taking the extreme example that the dip of the fault was 9.5° , 14.5° and 30° at the

eastern, central and western fans would yield total slip rates of $2.3 (\pm 0.6)$, $2.3 (\pm 0.3)$, and $2.2 (\pm 0.2)$ $\text{mm }^{10}\text{Be yr}^{-1}$, respectively.

4. The interplay of the timing of earthquakes and of fan abandonment could also cause some apparent variability in slip rates. Scarps ranging from 1 m to as high as 5 m have formed in association with roughly half of the major earthquakes in the Tien Shan: the 1812 Nilk earthquake, $M \sim 8$ (Feng, 1987; Yang et al., 1985); the 1842 earthquake, $M \sim 7.5$ (Feng Xianyue, 1985, personal commun.); the 1911 Chon-Kemin (or Kebin) earthquake, $M = 8.7$ (Bogdanovitch et al., 1914; Kuchai, 1969); the 1914 Barköl (Balikan He) earthquake, $M = 7.5$ (Feng Xianyue, 1985, personal commun.); and the 1992 Suusamyр earthquake, $M = 7.4$ (Ghose et al., 1997). Although much lower scarps, or none at all, have been assigned to other major earthquakes, we consider it reasonable that the scarps that we studied grow by jumps of 2 to 4 m in major earthquakes. If in the next few hundred years a major earthquake with a vertical component of slip of 3 m occurred, rates of slip deduced from the new scarps heights would be greater than those calculated here. The slip rate at the eastern fan would increase by 38% (to 0.51 ± 0.11 $\text{mm }^{10}\text{Be yr}^{-1}$ for the vertical component), but those of the central and western fans would increase by only 13% and 8%, respectively (to 0.65 ± 0.08 and 1.18 ± 0.12 $\text{mm }^{10}\text{Be yr}^{-1}$, for the vertical component), reducing the differences among the rates at the three sites.

At our site, because the geological blanks indicate relatively minor prior exposure, the oldest age from a given surface is likely to be the most accurate. We believe that the youngest surface, being the least affected by postdepositional processes, yields the best estimate for slip total rate: an upper limit of ~ 2 $\text{mm }^{10}\text{Be yr}^{-1}$.

SUMMARY AND CONCLUSIONS

We have demonstrated an approach for evaluating the extent of exposure to cosmic rays prior to deposition of material onto fans. At our study site, examination of rocks carried by currently active streams, and of material deposited on and buried in fans that were subsequently abandoned, indicates that surface exposure in source regions and during transport is limited to the equivalent of a few thousand years of ^{10}Be accumulation. This is small relative to the apparent ages of the fans, which range from 25 to 40 ka. These observations imply that the scatter in the cosmogenic nuclide contents of rocks at our study site is primarily due to postdepositional processes (erosion and burial) and that the calculated ages are lower limits. Accordingly, the sample with the oldest age for a given fan surface places a lower limit on

TABLE 1. ^{10}Be CONCENTRATIONS OF GEOLOGICAL BLANKS

Sample identification	^{10}Be (10^3 atom g^{-1})
Central fan	
Canyon walls	
TS93-29B	<2.8
TS93-29C	24.1 \pm 9.0
Active stream	
TS93-30C	16.8 \pm 9.5
TS93-30D	31.8 \pm 33.9
TS93-30F	14.1 \pm 8.1
Western fan	
Active stream	
TS93-70B	69.6 \pm 22.2
TS93-70D	57.7 \pm 19.9
TS93-70F	15.5 \pm 11.1
Eastern fan	
Active stream	
TS93-71B	31.6 \pm 17.0
TS93-71C	<10.3
TS93-71E	28.5 \pm 9.6

the age of abandonment and an upper limit on the slip rate of the fault that cuts the fan. Averaging ages from a collection of samples would underestimate the age of abandonment of the fan and overestimate the slip rate.

The oldest ages, 22 (± 5), 40 (± 9), and 35 (± 8) $\times 10^3$ calendar yr, for samples taken from each of the three fans provide lower limits for the time since abandonment of the surfaces. In central Asia, geomorphological events such as the deposition and subsequent abandonment of riverine fans have often been assumed to have occurred in conjunction with the termination of the last glacial maximum, ca. 10 to 15 ka; glacial meltwater was the source of the enhanced stream power necessary for incision and abandonment of fan surfaces. Assuming that fan abandonment was associated with incision due to enhanced stream power, these dates suggest that there may have been significant regional climatic events that did not occur synchronously with global glacial-interglacial cycles, consistent with observations that local alpine glaciers do not necessarily expand and retreat concurrently with global climatic cycles (Gillespie and Molnar, 1995). Furthermore, our results indicate that the abandonment of two of the three fans probably occurred during the last glacial period, and certainly occurred before its termination, supporting recent suggestions that not all prominent geomorphological features in arid Asian regions formed after the last glacial maximum (Molnar et al., 1994; Ritz et al., 1995).

The cosmic ray exposure dates provide lower limits for the time since abandonment of the fan surfaces and yield an upper limit of ~ 0.4 mm/yr for the rate of the vertical component of slip on the fault underlying the fans. This rate corresponds to an upper limit of ~ 2 mm/yr for the total slip rate at our site on the southern flank of the Tien Shan. This value is consistent with the low

TABLE 2. ^{10}Be CONCENTRATIONS AND APPARENT EXPOSURE AGES OF SAMPLES FROM THE THREE FANS

Sample identification	^{10}Be (10^3 atom g^{-1})	Apparent age* (10^3 ^{10}Be -yr)	Position on	
			East (m)	North (m)
Eastern fan				
TS93-37	355 \pm 35	21.5 \pm 2.7 [†]	1835	823
TS93-40	344 \pm 29	20.8 \pm 2.4	1823	786
TS93-41	253 \pm 23	14.8 \pm 2.1	1823	787
TS93-44	234 \pm 42	13.6 \pm 3.1	1914	945
TS93-45	239 \pm 19	13.9 \pm 1.9	1916	954
TS93-48	313 \pm 24	18.8 \pm 2.2	1945	934
Central fan				
TS93-21	281 \pm 55	16.6 \pm 3.9	667	1274
TS93-22	634 \pm 47	39.9 \pm 3.4	659	1315
TS93-23	535 \pm 40	33.4 \pm 3.0	698	1466
TS93-25	369 \pm 28	22.4 \pm 2.3	599	1615
TS93-33	390 \pm 63	23.8 \pm 4.3	543	999
TS93-34	434 \pm 45	26.7 \pm 3.3	613	993
Western fan				
TS93-51	250 \pm 34	16.3 \pm 2.7	130	127
TS93-54	332 \pm 40	22.3 \pm 3.4	142	119
TS93-55	357 \pm 32	24.2 \pm 2.8	180	139
TS93-56	498 \pm 40	34.5 \pm 3.4	316	238
TS93-58	372 \pm 33	25.3 \pm 2.9	321	367
TS93-64	323 \pm 36	21.7 \pm 3.1	459	569
TS93-67	503 \pm 38	34.9 \pm 3.2	271	694
TS93-68	353 \pm 40	23.9 \pm 3.4	346	578
TS93-69	344 \pm 24	23.2 \pm 2.4	346	580

*Corrected for exposure prior to deposition using the mean of the geological blanks ($25 \pm 21 \times 10^3$ atom g^{-1}).

[†]Uncertainties are based only on analytical errors.

end of the range (3 ± 1.5 mm/yr) inferred by Avouac et al. (1993) for the northern flank of the Tien Shan, and assumed by them to apply the south flank.

Although the rate of shortening across the Tien Shan in most areas is only poorly constrained, the sum of 3 ± 1.5 mm/yr for the northern flank and 2 mm/yr on the southern flank, $\sim 5 \pm 2$ mm/yr, appears to be too small. Recent geodetic measurements using Global Positioning System (GPS) satellites and receivers show 13 ± 2 mm/yr across $\sim 70\%$ of the belt ~ 1000 km to the west; extrapolation across the entire belt implies a current rate of ~ 20 mm/yr (Abdrakhmatov et al., 1996). The decreasing width of the Tien Shan from west to east and small paleomagnetic declination differences between the Tarim basin and Eurasia imply that the rate of convergence decreases eastward (Avouac et al., 1993). However, mapping of Quaternary deformation by Burchfiel et al. (in press) roughly 200 km west of where we worked indicates that there is between 4.5 and 14 mm/yr of shortening across the south flank of the Tien Shan. Although this 4.5 to 14 mm/yr rate is clearly less than 20 mm/yr, because it applies only to the southern margin of the Tien Shan, it is an underestimate for the entire cross section. Thus, the rate of 5 (± 2) mm/yr must underestimate shortening across the portion of the Tien Shan where we worked.

Such an inference follows from two other observations. First, active faults can be seen at the bases of individual ranges within the Tien Shan 100–200 farther east of where we worked,

though we are aware of no estimates of rates of slip for any of them. Second, the 1812 Nilk earthquake, which was assigned a magnitude of 8 and produced a high fresh scarp (Feng, 1987; Yang et al., 1985), occurred within the Tien Shan west of where we worked. Moreover, farther west, where GPS measurements have been made, deformation occurs throughout the Tien Shan (Abdrakhmatov et al., 1996; Makarov, 1977; Sadybasov, 1990). Thus, although we are aware of no definitive evidence for late Quaternary deformation within the interior of the Tien Shan between where we and Avouac et al. (1993) worked, the evidence from elsewhere in the belt makes such an inference sensible.

These qualitative arguments for shortening within the Tien Shan north of the terraces that we studied obscure a second aspect of deformation along the belt. The upper bound on the rate that we obtained for the southern margin of the Tien Shan is half the lower bound (4.5 mm/yr) that Burchfiel et al. (in press) inferred for the area 200–300 km west, where a fold-and-thrust belt has absorbed Quaternary convergence. Because the two studies consider very different intervals of time, less than 100 k.y. in this study and 2–3 m.y. by Burchfiel et al., part of the large difference might result from temporal changes in local rates of slip. Nevertheless, we suspect that the difference reflects real variations in the distribution of convergence along the belt. Whereas we studied faults bounding the range front, the northern flank of the Tien Shan north of where we worked is bounded by a fold-and-thrust belt, that

studied by Avouac et al. (1993) and also by Burchfiel et al. (in press). In contrast, 200 km to the west, the southern margin is bounded by a fold and thrust belt (where Burchfiel et al. [in press] estimated shortening to be 4.5 to 14 mm/yr), but the northern flank of the Tien Shan drops directly to the Dzhungarian basin, without such a belt. Thus, both the differences in rates and the differences in style imply that the distribution of convergence across cross sections varies along the Tien Shan; in some areas a large fraction of convergence is absorbed on one side or the other, and the importance of internal deformation within the belt also varies along it. Although the overall rate of shortening does not vary markedly from place to place, the distribution of shortening does, and this variation must reflect deeper processes that we do not yet understand.

ACKNOWLEDGMENTS

This research was supported in part by National Science Foundation grant EAR-9304587. We thank J. Lestringsuez and D. Deboffle for their expert assistance with the accelerator mass spectrometric measurements and M. W. Hamburger for help preparing Figure 1. Comments from E. J. Brook and reviews by P. Bierman, R. S. Anderson, and K. L. Prestegard improved the quality of this manuscript. Tandétron operation is supported by the Centre National de la Recherche Scientifique, Commissariat à l'Energie Atomique, and Institut National de Physique Nucléaire et de Physique des Particules.

REFERENCES CITED

- Abdrakhmatov, K. Ye., Aldazhanov, S. A., Hager, B. H., Hamburger, M. W., Herring, T. A., Kalabae, K. B., Makarov, V. I., Molnar, P., Panasyuk, S. V., Prilepin, M. T., Reilinger, R. E., Sadybakasov, I. S., Souter, B. J., Trapeznikov, Yu. A., Tsurkov, V. Ye., Zubovich, A. V., 1996, Relatively recent construction of the Tien Shan inferred from GPS measurements of present-day crustal deformation rates: *Nature*, v. 384, p. 450–453.
- Anderson, R. S., Repka, J. L., and Dick, G. S., 1996, Explicit treatment of inheritance in dating depositional surfaces using in situ ^{10}Be and ^{26}Al : *Geology*, v. 24, p. 47–51.
- Avouac, J. P., Tapponnier, P., Bai, M., You, H., and Wang, G., 1993, Active thrusting and folding along the northern Tien Shan, and late Cenozoic rotation of the Tarim relative to Dzhungaria and Kazakhstan: *Journal of Geophysical Research*, v. 98, p. 6755–6804.
- Bogdanovitch, K. I., Kark, I. M., Korolkov, B. Y., and Mushketov, D. I., 1914, The earthquake in the northern districts of the Tien Shan, 22 December 1910 (4 January 1911) (in Russian): St. Petersburg, Russia, Commission of the Geology Committee, 250 p.
- Brook, E. J., and Kurz, M. D., 1993, Surface-exposure chronology using in situ cosmogenic ^3He in Antarctic quartz sandstone boulders: *Quaternary Research*, v. 39, p. 1–10.
- Brown, E. T., Brook, E. J., Raisbeck, G. M., Yiou, F., and Kurz, M. D., 1992, Effective attenuation lengths of cosmic rays producing ^{10}Be and ^{26}Al in quartz: Implications for exposure age dating: *Geophysical Research Letters*, v. 19, p. 369–372.
- Burov, E. B., Kogan, M. G., Lyon-Caen, H., and Molnar, P., 1990, Gravity anomalies, the deep structure, and dynamic processes beneath the Tien Shan: *Earth and Planetary Science Letters*, v. 96, p. 367–383.
- Cerling, T. E., and Craig, H., 1994, Geomorphology and in-situ cosmogenic isotopes: *Annual Reviews of Earth and Planetary Science*, v. 22, p. 273–317.
- Clark, D. H., Bierman, P. R., and Larsen, P., 1995, Improving in situ cosmogenic chronometers: *Quaternary Research*, v. 44, p. 367–377.
- Ekström, G. A., 1987, A broad band method of earthquake analysis [Ph.D. dissert.]: Cambridge, Massachusetts, Harvard University, 219 p.
- Feng, X., 1987, Paleoseismological study of the Kaxhe fault zone, Xinjiang (in Chinese): *Seismology and Geology*, v. 9, p. 74–77.
- Feng, X., Deng, Q., Shi, J., Li, J., You, H., Zhang, Y., Yu, G., and Wu, Z., 1991, Active tectonics of the southern and northern Tianshan and its tectonic evolution (in Chinese), in *Research on active faults: Beijing, China, Seismological Press*, v. 1, p. 1–16.
- Ghose, S., Mellors, R. J., Hamburger, M. W., Pavlis, G. L., Pavlis, T. L., Korjenkov, A. M., Omuraliev, M., Mamyrov, E., and Muraliev, A. R., 1997, The Ms 7.3 1992 Suusamy, Kyrgyzstan, earthquake in the Tien Shan: 2. Aftershock focal mechanisms and surface deformation: *Bulletin of the Seismological Society of America*, v. 87, p. 23–38.
- Gillespie, A., and Molnar, P., 1995, Asynchronous maximal advances of mountain and continental glaciers: *Reviews of Geophysics*, v. 33, p. 311–364.
- Hanks, T. C., Bucknam, R. C., Lajoie, K. R., and Wallace, R. E., 1984, Modification of wave-cut and faulting-controlled landforms: *Journal of Geophysical Research*, v. 89, p. 5771–5790.
- Kuchai, V. K., 1969, Results of repeated examination of the remaining deformation in the pleistoseist of the Kebin earthquake (in Russian): *Geologiya i Geofizika*, p. 101–108.
- Lal, D., 1991, Cosmic ray labeling of erosion surfaces: In situ nuclide production rates and erosion models: *Earth and Planetary Science Letters*, v. 104, p. 424–439.
- Lal, D., and Arnold, J. R., 1985, Tracing quartz through the environment: *Proceedings of the Indian Academy of Sciences*, v. 94, p. 1–5.
- Makarov, V. I., 1977, New tectonic structures of the Central Tien Shan (in Russian): Moscow, Academy of Sciences, Order of the Red Banner Geology Institute, Transactions, 171 p.
- Makeyeva, L. I., Vinnik, L. P., and Roecker, S. W., 1992, Shear-wave splitting and small-scale convection in the continental upper mantle: *Nature*, v. 358, p. 144–147.
- Molnar, P., and Deng, Q., 1984, Faulting associated with large earthquakes and the average rate of deformation in central and eastern Asia: *Journal of Geophysical Research*, v. 89, p. 6203–6227.
- Molnar, P., Brown, E. T., Burchfiel, B. C., Deng, Q., Feng, X., Li, J., Raisbeck, G. M., Shi, J., Wu, Z., Yiou, F., and You, H., 1994, Quaternary climate change and the formation of river terraces across growing anticlines on the North Flank of the Tien Shan, China: *Journal of Geology*, v. 102, p. 583–602.
- Nelson, M. R., McCaffrey, R., and Molnar, P., 1987, Source parameters for 11 earthquakes in the Tien Shan, Central Asia, determined by P and SH waveform inversion: *Journal of Geophysical Research*, v. 92, p. 12629–12648.
- Ni, J., 1978, Contemporary tectonics in the Tien Shan region: *Earth and Planetary Science Letters*, v. 41, p. 347–355.
- Nishiizumi, K., Winterer, E. L., Kohl, C. P., Klein, J., Middleton, R., Lal, D., and Arnold, J. R., 1989, Cosmic ray production rates of ^{10}Be and ^{26}Al in quartz from glacially polished rocks: *Journal of Geophysical Research*, v. 94, p. 17907–17915.
- Raisbeck, G. M., Yiou, F., Bourlès, D., Lestringsuez, J., and Deboffle, D., 1987, Measurements of ^{10}Be and ^{26}Al with a Tandetron AMS facility: Nuclear Instruments and Methods in Physics Research, v. B29, p. 22–26.
- Raisbeck, G. M., Yiou, F., Bourlès, D., Brown, E., Deboffle, D., Jouhannau, P., Lestringsuez, J., and Zhou, Z. Q., 1994, The AMS facility at Gif-sur-Yvette: Progress, perturbations and projects: *Nuclear Instruments and Methods in Physics Research*, v. B92, p. 43–46.
- Richter, C. F., 1958, *Elementary seismology*: San Francisco, W. H. Freeman, 768 p.
- Ritz, J. F., Brown, E. T., Bourlès, D. L., Philip, H., Schlupp, A., Raisbeck, G. M., Yiou, F., and Enkvtshin, B., 1995, Slip rates along active faults estimated with cosmic-ray exposure dates: Application to the Bogd fault, Gobi-Altai, Mongolia: *Geology*, v. 23, p. 1019–1022.
- Roecker, S. W., Sabitova, T. M., Vinnik, L. P., Burmakov, Y. A., Golvanov, M. I., Matatkanova, R., and Munirova, L., 1993, Three-dimensional elastic wave velocity structure of the western and central Tien Shan: *Journal of Geophysical Research*, v. 98, p. 15779–15795.
- Sadybakasov, I., 1990, *Neotectonics of High Asia* (in Russian): Moscow, Nauka, 176 p.
- Shirokova, E. I., 1967, General regularities in the orientation of principal stresses in the foci of earthquakes of the Mediterranean-Asiatic seismic belt (in Russian): *Izvestiya Akademiyi Nauk, USSR, Physics of the Solid Earth*, v. 1, p. 23–36.
- Shirokova, E. I., 1974, Detailed study of the stresses and fault planes at earthquake foci of Central Asia (in Russian): *Izvestiya Akademiyi Nauk, USSR, Physics of the Solid Earth*, v. 11, p. 22–36.
- Tapponnier, P., and Molnar, P., 1979, Active faulting and Cenozoic tectonics of the Tien Shan, Mongolia and Baykal Regions: *Journal of Geophysical Research*, v. 84, p. 3425–3459.
- Terman, M. J., Woo, C. C., Alverson, D. C., Cox, D. P., and Woloshin, A. J., 1967, To support detection of underground nuclear explosions, in *Atlas of Asia and Eastern Europe to support detection of underground nuclear testing*: Reston, Virginia, U.S. Geological Survey, 24 p.
- 385Yang, Z., Zhang, Y., Li, J., and Yin, G., 1985, A preliminary study of the originating tectonics of the Nilk earthquake ($M = 8$) in Xinjiang, of March 8, 1812: *Acta Seismologica Sinica*, v. 7, p. 434–444.
- Yiou, F., Raisbeck, G. M., Klein, J., and Middleton, R., 1984, $^{26}\text{Al}/^{10}\text{Be}$ in terrestrial impact glasses: *Journal of Non-Crystalline Solids*, v. 67, p. 503–509.

MANUSCRIPT RECEIVED BY THE SOCIETY APRIL 19, 1996

REVISED MANUSCRIPT RECEIVED DECEMBER 11, 1996

MANUSCRIPT ACCEPTED MAY 20, 1997